Multi-fidelity wing aerostructural optimization using a trust region filter-SQP algorithm

Elham, Ali; van Tooren, Michel

DOI
10.1007/s00158-016-1613-0

Publication date
2016

Document Version
Final published version

Published in
Structural and Multidisciplinary Optimization

Struct Multidisc Optim
DOI 10.1007/s00158-016-1613-0

RESEARCH PAPER

Multi-fidelity wing aerostructural optimization using a trust region filter-SQP algorithm

Ali Elham[1] · **Michel J. L. van Tooren**[2]

Received: 10 May 2016 / Revised: 16 October 2016 / Accepted: 26 October 2016

Abstract A trust region filter-SQP method is used for wing multi-fidelity aerostructural optimization. Filter method eliminates the need for a penalty function, and subsequently a penalty parameter. Besides, it can easily be modified to be used for multi-fidelity optimization. A low fidelity aerostructural analysis tool is presented, that computes the drag, weight and structural deformation of lifting surfaces as well as their sensitivities with respect to the design variables using analytical methods. That tool is used for a mono-fidelity wing aerostructral optimization using a trust region filter-SQP method. In addition to that, a multi-fidelity aerostructural optimization has been performed, using a higher fidelity CFD code to calibrate the results of the lower fidelity model. In that case, the lower fidelity tool is used to compute the objective function, constraints and their derivatives to construct the quadratic programming subproblem. The high fidelity model is used to compute the objective function and the constraints used to generate the filter. The results of the high fidelity analysis are also used to calibrate the results of the lower fidelity tool during the optimization. This method is applied to optimize the wing of an A320 like aircraft for minimum fuel burn. The results showed about 9 % reduction in the aircraft mission fuel burn.

Keywords Aerostructural optimization · Multi-fidelity optimization · Trust region filter-SQP algorithm

This paper has been modified from A.Elham and M.J.L. van Tooren, "Trust region filter-SQP method for multi-fidelity wing aerostructural optimization", Variational analysis and aerospace engineering III workshop, August 28 - September 5, 2015, Erice, Italy.

✉ Ali Elham
a.elham@tudelft.nl

Michel J. L. van Tooren
vantooren@cec.sc.edu

[1] Faculty of Aerospace Engineering, Delft University of Technology, Kluyverweg 1, 2629HS, Delft, Netherlands

[2] McNair Center for Aerospace Research and Innovation, University of South Carolina, Columbia, SC, 29208, USA

1 Introduction

According to industry criteria for aircraft design, the drag prediction accuracy using numerical methods should be within one drag count (one ten thousandth of the drag coefficient) (van Dam 2003). To confirm a need for such a level of accuracy, Meredith (1993) showed that changing the drag coefficient by 0.0001 has an effect equivalent to the weight of one passenger for a long-haul aircraft. Similarly, one percent error in wing structural weight estimation of the same class aircraft is equal to the weight of 4 to 5 passengers. The need for such a high level of accuracy forces the designers to use high fidelity, physics based analysis for aerostructural analysis, design and optimization of aircraft. The traditional design methods based on empirical, statistic based methods do not satisfy the required level of accuracy.

On the other hand, using high fidelity methods for aerostructural optimization requires massive computational power (Kenway and Martins 2014; Kennedy and Martins 2014), that is a serious barrier against using high fidelity aerostructural optimization in early design stages. As a

Published online: 23 November 2016

solution multi-fidelity optimization techniques are used to keep the level of accuracy similar to the results of the high fidelity analysis methods, while reduce the computational cost of the optimization. Alexandrov et al. (2001) presented a model management framework for multi-fidelity aerodynamic shape optimization of lifting surfaces based on a trust region algorithm. In that model a lower fidelity tool is used for the optimization, while a higher fidelity tool is occasionally, but systematically, called to monitor the optimization process. March and Willcox (2010) suggested a multi-fidelity optimization framework based on a trust region algorithm, in which the gradient of the objective function is computed using the low fidelity model, but the algorithm is provably convergent to the solution of the high fidelity model. The same algorithm is used by Elham (2015) for aerodynamic shape optimization of lifting surfaces, where an adjoint quasi-three-dimensional (Q3D) model is used for prediction of the wing drag and its derivatives, and a three-dimensional CFD tool is used to calibrate the results of the Q3D model. Applications of multi-fidelity model-based strategy for aerodynamic and aerostructural optimization are presented by Rajnarayan et al. (2008) and Berci et al. (2014).

Besides the framework for model management in a multi-fidelity optimization, the choice of a proper algorithm for numerical optimization is important. Aerostructural optimization of lifting surfaces, or the whole aircraft in general, involves hundreds to thousands of design variables, and tens to hundreds of constraints. Besides, computing the objective function and the constraints required execution of CFD and FEM analysis, which takes considerable amount of time. Therefore the gradient based optimization algorithms are the most efficient algorithms for solving such problems (Martins et al. 2005). In an optimization using a gradient based algorithm, in order to achieve a quadratic rate of convergence, an underlying Newton iteration is required, which is the basics of Sequential Quadratic Programming (SQP). The SQP algorithms are based on iteratively solving a quadratic model of the objective function and linear models of the constraints. The SQP approach has been used in both line search and trust region frameworks (Nocedal and Wright 2000). Many of the SQP methods use a penalty function, which combines the objective function and the constraints. An ℓ_1 penalty function and the augmented Lagrangian function are popular choices for the penalty function. Selection of a proper penalty function, and the method used for updating the penalty parameter is a challenge (Nocedal and Wright 2000). Fletcher and Leyffer (2002) proposed a method to eliminate the need for a penalty function in an SQP algorithm. They suggested a *filter* that rejects the unacceptable solutions. In that so-called *trust region filter-SQP algorithm*, no penalty function is constructed and the filter is applied to the objective function and the (norm of the) constraints separately.

In this research a modified version of the filter method proposed by Fletcher and Leyffer is applied to multi-fidelity aerostructural optimization of lifting surfaces. In the next section, the aerostructural analysis tool used in this research is briefly explained. Then in Section 3, the trust region filter-SQP method is discussed in detail. Eventually in Section 4 the filter method is applied to both a mono-fidelity and a multi-fidelity wing aerostructural optimization.

2 Aerostructural analysis

The FEMWET tool presented by Elham and van Tooren (2016b) is used for wing aerostructural analysis. FEMWET is based on a Q3D aerodynamic analysis method, which is combined with a finite beam element model of the structure. In the Q3D approach an inviscid vortex lattice method (VLM) is combined with a viscous 2D airfoil analysis code for prediction of the wing total viscous drag. The idea behind the Q3D approach is to avoid using a high fidelity 3D CFD solver, but still predict drag with the same level of accuracy. In the proposed method the wing drag is decomposed into the induced drag and the parasite drag. To compute the wing total drag, first a VLM is executed to compute the lift distribution over the wing as well as the wing induced drag using a Trefftz plane analysis. The VLM code is connected to a FEM to automatically deform the VLM mesh based on the wing structural deformation. Then several sections along the span are analyzed using a 2D airfoil analysis CFD code. The parasite drag is computed based on the pressure and friction drag of the 2D sections. In order to perform the 2D analysis, several corrections, including the corrections due to sweep, induced angle of attack and wing structural deformation are applied to the section geometry as well as the flow conditions. Details of this method are presented in reference (Elham and van Tooren 2016b).

The wing box structure is modeled using four equivalent panels: the upper panel, including the wing box upper skin, stringers and spars caps; the lower panel including the lower skin,stringers and spar caps; and two vertical panels including the front and the rear spars webs. The stiffened panel efficiency method presented by Niu (1997) is used to model the effect of stringers on the thickness of the equivalent panels. For finite element analysis of the wing box structure an equivalent Timoshenko beam is placed at the shear center of the wing box, see Fig. 1. Using this FEM model different failure criteria, referred to tension, compression, Euler buckling and shear buckling in several wing box elements, located in (y_e, z_e) distance from the shear center (see Fig. 1), are calculated. For more details one can refer to Elham and van Tooren (2016b).

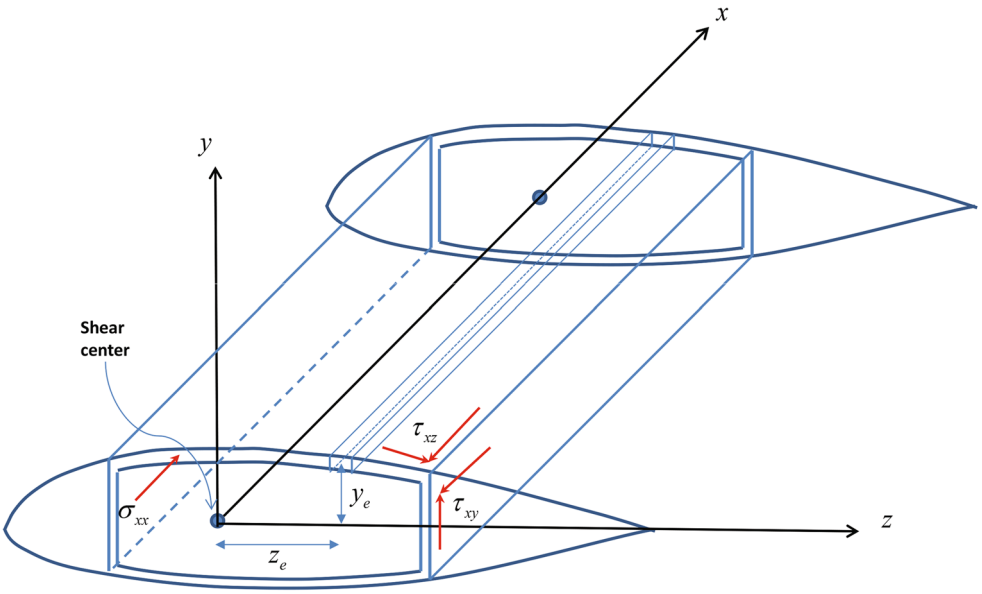

Fig. 1 Wing box panels element position w.r.t the shear center

When the Q3D aerodynamic solver is combined with the finite beam element model, four governing equations appear as follows:

$$R_1(X, \Gamma, U, \alpha, \alpha_i) = AIC\ \Gamma - RHS = 0 \tag{1}$$

$$R_2(X, \Gamma, U, \alpha, \alpha_i) = KU - F = 0 \tag{2}$$

$$R_3(X, \Gamma, U, \alpha, \alpha_i) = L - nW_{des} = 0 \tag{3}$$

$$R_4(X, \Gamma, U, \alpha, \alpha_i) = C_{l_{2d}} - C_{l_{vlm}} = 0 \tag{4}$$

The first equation is the governing equation of the VLM and the second equation is the governing equation of the FEM. The third equation in fact indicates that the lift should be equal to the design weight multiplied by the load factor. The last equation is required to guarantee that the lift predicted by the VLM is the same as the lift computed by 2D section analysis at effective angle of attack. The effective angle of attack is the angle of attack that a 2D local section feels. Therefore the local downwash angle is required to compute the effective angle of attack. In such a system four sets of state variables are presented: the strengths of vortices in the VLM (Γ), the displacements in FEM (U), the global angle of attack (α) and the local downwash angles at each 2D section (α_i). For a given vector of design variables, X, the system of governing equations are solved using the Newton method:

$$\underbrace{\begin{bmatrix} \frac{\partial R_1}{\partial \Gamma} & \frac{\partial R_1}{\partial U} & \frac{\partial R_1}{\partial \alpha} & \frac{\partial R_1}{\partial \alpha_i} \\ \frac{\partial R_2}{\partial \Gamma} & \frac{\partial R_2}{\partial U} & \frac{\partial R_2}{\partial \alpha} & \frac{\partial R_2}{\partial \alpha_i} \\ \frac{\partial R_3}{\partial \Gamma} & \frac{\partial R_3}{\partial U} & \frac{\partial R_3}{\partial \alpha} & \frac{\partial R_3}{\partial \alpha_i} \\ \frac{\partial R_4}{\partial \Gamma} & \frac{\partial R_4}{\partial U} & \frac{\partial R_4}{\partial \alpha} & \frac{\partial R_4}{\partial \alpha_i} \end{bmatrix}}_{J} \begin{bmatrix} \Delta\Gamma \\ \Delta U \\ \Delta\alpha \\ \Delta\alpha_i \end{bmatrix} = - \begin{bmatrix} R_1(X, \Gamma, U, \alpha, \alpha_i) \\ R_2(X, \Gamma, U, \alpha, \alpha_i) \\ R_3(X, \Gamma, U, \alpha, \alpha_i) \\ R_4(X, \Gamma, U, \alpha, \alpha_i) \end{bmatrix} \tag{5}$$

To perform the Newton iteration, the matrix of the partial derivatives J is required. All the elements of that matrix are computed by a combined use of analytical methods and Automatic Differentiation (AD). The Matlab toolbox Intlab (Rump 1999) is used for AD. More details of the sensitivity analysis are presented in Elham and van Tooren (2016b). In order to compute the sensitivity of the output (e.g. wing drag or structural failure loads) the coupled adjoint method (Kenway et al. 2014) is used, where the total derivative of any function of interest I, with respect to a design variable x is presented as follows:

$$\frac{dI}{dx} = \frac{\partial I}{\partial x} - \lambda_1^T \left(\frac{\partial R_1}{\partial x}\right) - \lambda_2^T \left(\frac{\partial R_2}{\partial x}\right) - \lambda_3^T \left(\frac{\partial R_3}{\partial x}\right) - \lambda_4^T \left(\frac{\partial R_4}{\partial x}\right) \tag{6}$$

in which $\lambda = [\lambda_1 \quad \lambda_2 \quad \lambda_3 \quad \lambda_4]^T$ is the adjoint vector and computed using the following equation:

$$\begin{bmatrix} \frac{\partial R_1}{\partial \Gamma} & \frac{\partial R_1}{\partial U} & \frac{\partial R_1}{\partial \alpha} & \frac{\partial R_1}{\partial \alpha} \\ \frac{\partial R_2}{\partial \Gamma} & \frac{\partial R_2}{\partial U} & \frac{\partial R_2}{\partial \alpha} & \frac{\partial R_2}{\partial \alpha} \\ \frac{\partial R_3}{\partial \Gamma} & \frac{\partial R_3}{\partial U} & \frac{\partial R_3}{\partial \alpha} & \frac{\partial R_3}{\partial \alpha} \\ \frac{\partial R_4}{\partial \Gamma} & \frac{\partial R_4}{\partial U} & \frac{\partial R_4}{\partial \alpha} & \frac{\partial R_4}{\partial \alpha} \end{bmatrix}^T \begin{bmatrix} \lambda_1 \\ \lambda_2 \\ \lambda_3 \\ \lambda_4 \end{bmatrix} = \begin{bmatrix} \frac{\partial I}{\partial \Gamma} \\ \frac{\partial I}{\partial y} \\ \frac{\partial I}{\partial \alpha} \\ \frac{\partial I}{\partial \alpha_i} \end{bmatrix} \tag{7}$$

The FEMWET tool is also able to compute the aileron effectiveness and its sensitivity with respect to the design variables. The aileron effectiveness is defined as $L_{\delta_{\text{elastic}}}/L_{\delta_{\text{rigid}}}$. The parameter L_δ is the derivative of the wing rolling moment w.r.t the aileron deflection angle. This parameter is an important requirement for aircraft performance and is strongly affected by the wing stiffness. Low wing (mainly torsional) stiffness may result in a poor

roll performance or even aileron reversal. Therefore for a wing aerostructural optimization a constraint on the aileron effectiveness seems necessary.

Elham and van Tooren (2016b) performed some analysis and aerostructural optimization to verify the results of the FEMWET tool. In order to verify the accuracy of the wing drag prediction, the results of Q3D aerodynamic solver were compared to the results of a higher fidelity CFD code called MATRICS-V (van der Wees et al. 1993). The MATRICS-V flow solver is based on fully conservative full potential outer flow in quasi-simultaneous interaction with an integral boundary layer method on the wing. The MATRICS-V tool was developed by NLR and has been validated using wind tunnel test as well as the flight test results for Fokker 100 aircraft, see Figs. 2 and 3. Therefore the drag of the Fokker 100 wing predicted by the Q3D solver was compared to the drag predicted by MATRICS-V, see Fig. 4. From this figure one can observe a high level of accuracy for drag prediction using the Q3D solver.

In order to validate the wing weight and structural deformation predicted by FEMWET, Elham and van Tooren (2016b) performed an aeroelastic wingbox optimization of Airbus A320-200 wing. The optimization included five different load cases to evaluate the structural failure with respect to tensile and compressive loads, buckling, fatigue and aileron effectiveness. The total wing weight predicted by FEMWET is equal to 8791kg, which is very close to the actual wing weight of A320-200 equal to 8801kg (Obert 2009). The wing twist deformation predicted by FEMWET was compared to the actual wing twist deformation under 1g load (obtained from Obert (2009)). Figure 5 shows the the wing actual twist distribution (including the wing incidence angle at the wing root) compared to the computed values. The results show an acceptable level of accuracy for the tool.

3 Trust region filter-SQP method

A general optimization problem is defined as follows:

$$\begin{aligned} \text{minimize} \quad & f(x) \\ s.t. \quad & c(x) = 0 \end{aligned} \tag{8}$$

Only equality constraints are considered here, however inequality constraints can be defined as equality constraints using slack variables and adding simple bounds, see Nocedal and Wright (2000). Using an SQP approach, (8) is solved by solving the following quadratic problem (QP) iteratively:

$$\begin{aligned} \text{minimize} \quad & \frac{1}{2}\, s^T H(x_k)\, s + g(x_k)^T s \\ s.t. \quad & c(x_k) + A(x_k)s = 0 \end{aligned} \tag{9}$$

where H is the Hessian matrix of the Lagrangian function, g and A are the gradient of the objective function and the constraints respectively. Most of the available SQP algorithms use the solution of the QP as a search direction, then find a step length that minimizes a one-dimensional problem, which results in a sufficient decrease of a penalty function. The penalty function combines the objective function and the constraints in a single function. One-dimensional optimization algorithms, (such as polynomial interpolation) (Vanderplaats 2007) or line search algorithms (Nocedal and Wright 2000) are used to find the step length. An alternative to this approach is the use of trust region algorithms (Conn et al. 2000). Trust region methods define a region

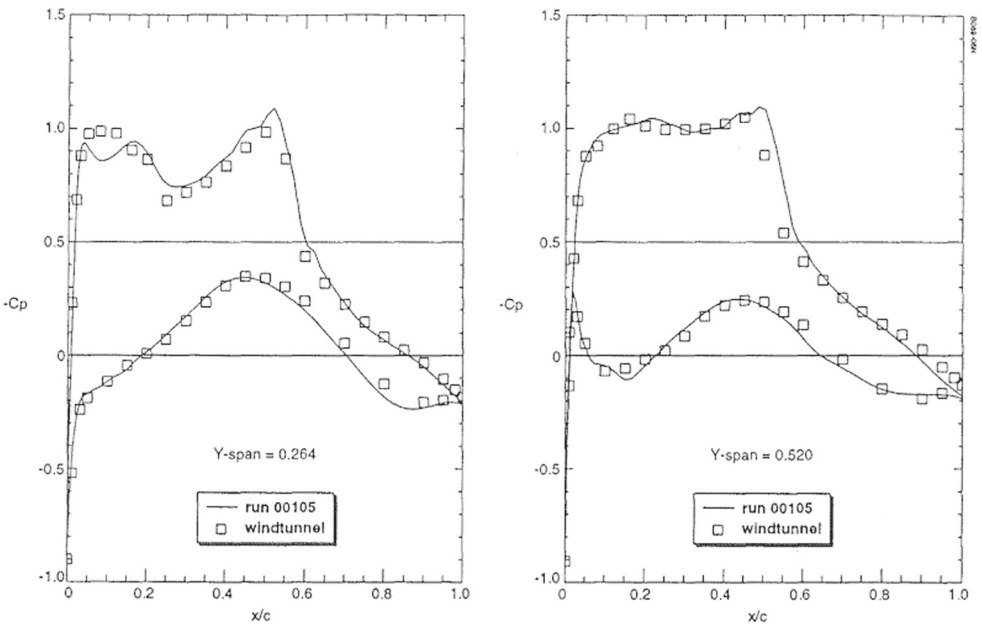

Fig. 2 Comparison of MATRICS-V and wind tunnel measured chordwise pressure distribution on two wing sections of Fokker 100 wing/body configuration at $M_\infty = 0.779$, $\alpha = 1.03°$, $Re_\infty = 3 \times 10^6$. Source: NLR (van der Wees et al. 1993)

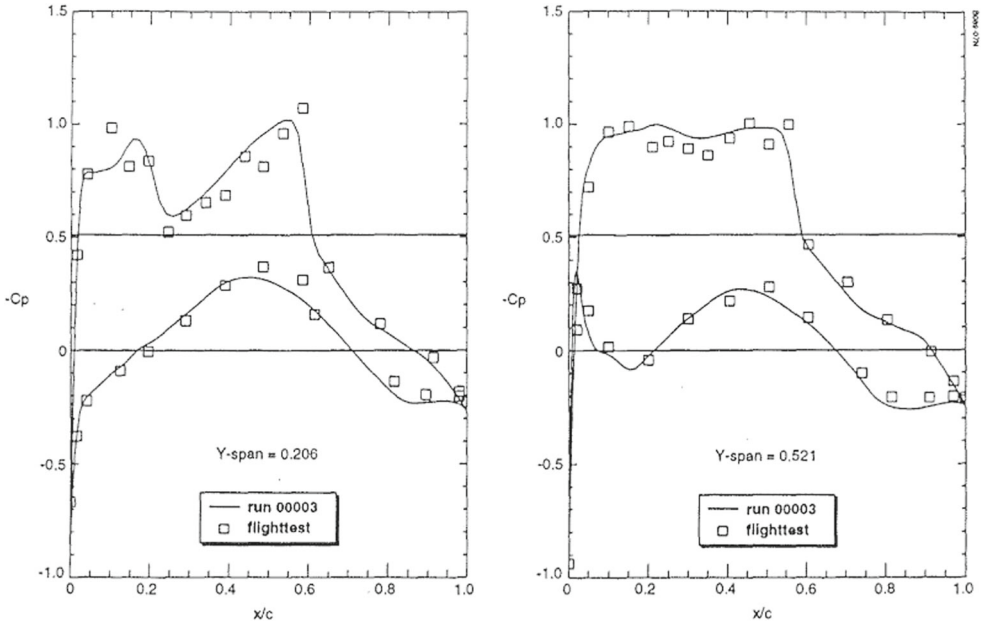

Fig. 3 Comparison of MATRICS-V and in flight measured chordwise pressure distribution on two wing sections of Fokker 100 wing/body configuration at $M_\infty = 0.775$, $\alpha = 1.0°$, $Re_\infty = 35 \times 10^6$. Source: NLR (van der Wees et al. 1993)

around the current point, where the approximations of the objective function and constraints are trusted. The radius of the trust region plays the role of the step length, so the trust region algorithms find the search direction and the step length simultaneously. However the need for a penalty function is still there.

As mentioned earlier, definition of a penalty function and consequently a method for updating an associated penalty parameter is a challenge. Some aspects of the difficulties associated with the choice of the penalty function and the penalty parameter are discussed in Fletcher and Leyffer (2002). The filter method presented by Fletcher and Leyffer (2002) eliminates the need for a penalty function in an SQP algorithm. The concept of the filter is based on the two goals of a constrained optimization problem: minimizing the objective function and minimizing the constraint violation. So in the method proposed by Fletcher and Leyffer a filter is used to only accept the solutions that are not dominated by the Pareto front between the objective function and the constraint violation, see Fig. 6. If ϑ is the 2-norm of the (equality) constraints, the pair (f_1, ϑ_1) is said to dominate (f_2, ϑ_2) if and only if both $f_1 \leq f_2$ and $\vartheta_1 \leq \vartheta_2$. Defining $\mathcal{F}$ as the filter, that includes a set of pairs (f_j, ϑ_j) such that no pair dominate any other, a pair (f, ϑ) is acceptable to $\mathcal{F}$ if it is not dominated by any pair in the filter.

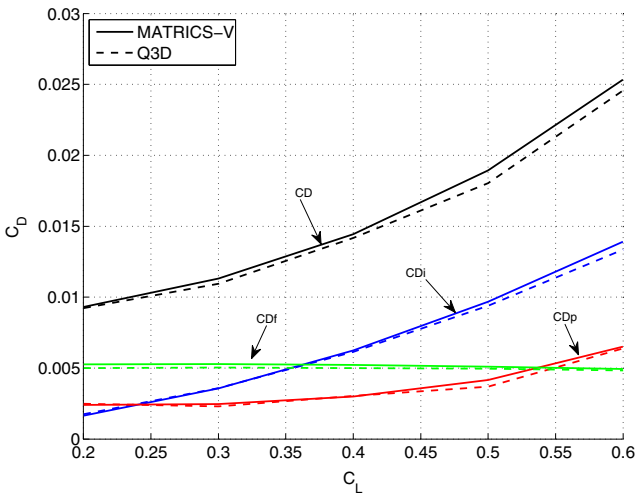

Fig. 4 Comparison of computed drag by the MATRICS-V and Q-3D solvers for cruise condition (1g loaded wing and M = 0.75) (Elham and van Tooren 2016b)

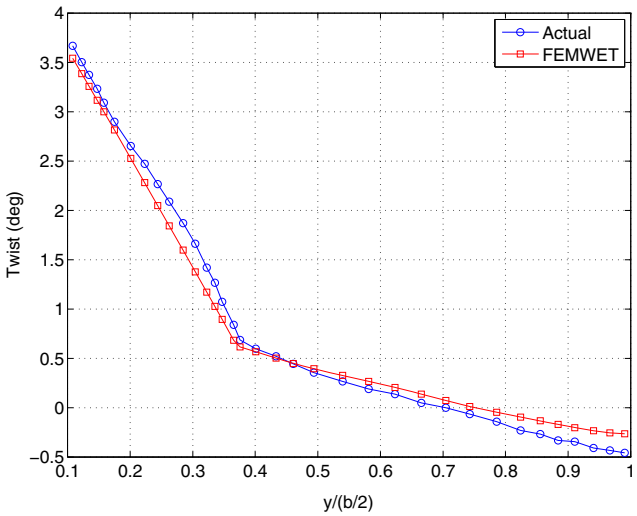

Fig. 5 A320-200 wing twist under 1g load (Elham and van Tooren 2016b)

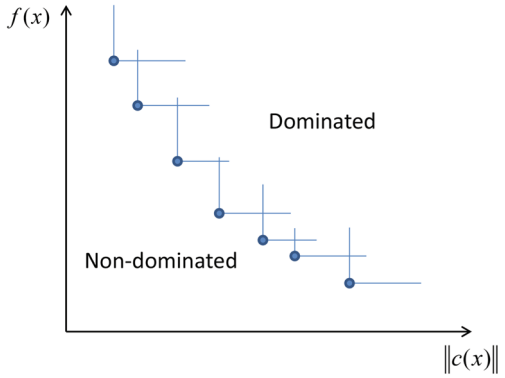

Fig. 6 Dominated and non-dominated points according to the filter

In a trust region filter-SQP method, the QP shown in (9) is solved within a trust region, then the solution is checked by the filter. If the filter rejects the solution, the radius of the trust region is reduced, see Fletcher and Leyffer (2002) for more details. A common problem in trust region methods, is that the QP may have no feasible solution if the radius of the trust region is small. In such cases a constraint *restoration* is required. The idea of constraint restoration is to minimize $\vartheta(x)$ starting from the current iteration. A basic trust region filter-SQP algorithm in shown in Algorithm 1.

Algorithm 1 Basic trust region filter-SQP algorithm

1: Choose x_0, Δ_0 and set $k = 0$
2: Solve the trust region quadratic problem (TRQP):

$$\begin{aligned} \text{minimize} \quad & \frac{1}{2} s^T H(x_k)\, s + g(x_k)^T s \\ s.t. \quad & c(x_k) + A(x_k)s = 0 \\ & \|s\| \le \Delta_k \end{aligned}$$

3: if TRQP is infeasible perform a constraint restoration (see Algorithm 2) and go to 2, otherwise continue.
4: set $x_{k+1} = x_k + s$
5: if $(f(x_{k+1}), \vartheta(x_{k+1}))$ is acceptable to the filter, then accept x_{k+1}, add $(f(x_{k+1}), \vartheta(x_{k+1}))$ to the filter, remove the dominated points from the filter and increase the trust region radius if possible. Else reject x_{k+1} and reduce the trust region radius.
6: if the solution is not converged go to 2.

In order to prove the convergence of the trust region filter-SQP algorithm, a small envelope is required around the current filter, in which no point is accepted. This envelope in fact enforces a sufficient decrease in the objective function and the constraint. According to Fletcher et al. (2002) a point is acceptable to the filter if:

$$\text{either} \quad f \le f_j - \gamma \vartheta_j \quad \text{or} \quad \vartheta \le \beta \vartheta_j \quad \text{for all j} \in \mathscr{F} \quad (10)$$

The proof of convergence of such an algorithm is given in Fletcher et al. (2002). A more refined trust region filter-SQP method is presented by Conn et al. (2000), although in that algorithm a composite step optimization is used, where first in a normal step the norm of the constraints is minimized within the trust region and then in a tangential step the objective function is reduced. In this research the algorithm presented in Conn et al. (2000) is modified to use the original SQP method presented by Fletcher and Leyffer (2002) instead of a composite step optimization. This algorithm is presented in Algorithm 2.

Algorithm 2 Trust region filter-SQP method

1: Choose x_0, Δ_0, Δ_{max}, Δ_{min}, η_1, η_2, γ_0, γ_1, γ_ϑ, k_ϑ
2: Initialize the Hessian as $H_0 = I$
3: Compute the value and the gradient of the objective function and the constraints.
4: Solve the trust region quadratic programming (TRQP) to find s:

$$\begin{aligned} \text{minimize} \quad & m_k(s) = \frac{1}{2} s^T H(x_k)\, s + g(x_k)^T s \\ s.t. \quad & c(x_k) + A(x_k)s = 0 \\ & |s| \le \Delta_k \end{aligned}$$

5: If the TRQP does not have a feasible solution, then solve the restoration problem:

$$\text{minimize} \quad \vartheta(x_k + s) \equiv \|c(x_k + s)\|$$

6: Evaluate the objective function and the constraints at $x_k + s$.
7: Check if the new point is acceptable to the filter, i.e. if:

$$f(x_k + s_k) < f_j - \gamma_\vartheta \vartheta(x_k + s_k) \quad \text{or}$$
$$\vartheta(x_k + s_k) < (1 - \gamma_\vartheta)\vartheta_j \quad \text{for all } (f_j, \vartheta_j) \in \mathscr{F}$$

8: If $x_k + s_k$ is not acceptable to the filter, then set $x_{k+1} = x_k$ and $\Delta_{k+1} = min(\Delta_{min}, \gamma_0 \Delta_k)$ and go to 4.
9: If $x_k + s_k$ is acceptable to the filter and:

$$m_k(x_k) - m_k(x_k + s_k) < k_\vartheta \vartheta_k^2 \quad \text{and}$$
$$\rho_k \equiv \frac{f(x_k) - f(x_k + s_k)}{m_k(x_k) - m_k(x_k + s_k)} \ge \eta_1$$

then set $x_{k+1} = x_k + s_k$, update the Hessian using i.e. the BFGS method and continue, else set $x_{k+1} = x_k$ and $\Delta_{k+1} = min(\Delta_{min}, \gamma_0 \Delta_k)$ and go to 4.
10: Add F_k and ϑ_k to the filter, remove the dominated pairs and update the trust region radius as follows:

$$\Delta_{k+1} = \begin{cases} \Delta_k & \text{if } \rho_k \in [\eta_1, \eta_2), \\ max(\Delta_{max}, \gamma_1 \Delta_k) & \text{if } \rho_k \ge \eta_2. \end{cases}$$

11: If the optimization has not converged go to 3.

Conn et al. (2000) suggested the following values for the constants in Algorithm 2:

$$\gamma_0 = 0.5 \quad \gamma_1 = 2 \quad \eta_1 = 0.01 \quad \eta_2 = 0.9$$
$$\gamma_\vartheta = 10^{-4} \quad k_\vartheta = 10^{-4}$$

In some of the trust region methods, as in the one suggested by Conn et al. (2000), a ℓ_2 trust region subproblem is used. However in the filter method suggested by Fletcher and Leyffer (2002) a ℓ_∞ trust region subproblem is used to ensure that the subproblem remains tractable as a QP. In this research instead of ℓ_2 or ℓ_∞, the trust region is defined to keep the absolute value of s lower than the trust region radius, see Algorithm 2. It has an advantage when the algorithm is applied to a wing aerostructural optimization. This advantage is explained in Section 4. In such an approach the trust region for a 2D case is a rectangle instead of a circle for ℓ_2 or a square for ℓ_∞.

To check the algorithm an analytical optimization test case is used as follows:

$$\begin{aligned} min \quad & e^{x_1 x_2 x_3 x_4 x_5} \\ s.t. \quad & x_1^2 + x_2^2 + x_3^2 + x_4^2 + x_5^2 - 10 = 0 \\ & x_2 x_3 - 5 x_4 x_5 = 0 \\ & x_1^3 + x_2^3 + 1 = 0 \\ & lb \le x \le ub \\ & ub = [2.3, 2.3, 3.2, 3.2, 3.2], \quad lb = -ub \end{aligned} \tag{11}$$

The global minimum for this function is $x^* = [-1.717143, 1.595709, 1.827247, -0.7636413, -0.763645]$, $f(x^*) = 0.0539498$. The optimization was started from an initial point of $x_0 = [1, 1, 1, 1, 1]$ and the proposed filter method found the optimum design vector of $x^* = [-1.7171, 1.5957, 1.8273, -0.7636, -0.7636]$ and $f(x^*) = 0.0539$. The history of the objective function and norm of the constraints are shown in Fig 7.

4 Wing aerostructural optimization

4.1 Problem formulation

An A320 like aircraft wing is considered as a test case, see Fig. 8. The aircraft mission fuel weight is considered as the objective function. It is computed using the method presented by Roskam (1986). In that method the fuel weight of the cruise phase of the flight is computed using the Breguet method, and the fuel weights of the other segments of the mission, e.g. take-off, climb, etc. are computed using some statistical factors. In order to use the Breguet equation, the aircraft lift over drag ratio during the cruise is required. The lift and drag of the elastic wing during the cruise is computed using the FEMWET for an average aircraft all up weight equal to $W_{ave} = \sqrt{MTOW \times (MTOW - W_{fuel})}$ as suggested by Torenbeek (2013). The drag of the other aircraft components such as fuselage, tail etc. is assumed to be constant.

The design variables are categorized into four groups. The first group includes the design variables describing the wing planform geometry. Six design variables are used for that purpose: the wing root chord C_r, span b, taper ratio λ, leading edge sweep angle Λ, twist angle at kink ϵ_k and twist angle at tip ϵ_t. The wing aileron geometry was defined using three parameters. The start and end position of the aileron was fixed at 75 % and 95 % of the wing span. The aileron chord was fixed as 25 % of the local wing chord. The second group of design variables defines the wing airfoil shape. In order to reduce the number of design variables and guarantee a smooth shape for the airfoil, the airfoil shape is parametrized using the Chebychev polynomials. The Chebychev polynomials, g_i, are defined as:

$$g_j(x) = cos\left(j\ cos^{-1}(x)\right) \tag{12}$$

Using the Chebychev polynomials the original airfoil shape is perturbed as:

$$\Delta n(s) = \sum_{j=1}^{J} G_j\ g_j(s) \tag{13}$$

where Δn is the airfoil perturbation normal to its current surface, s is the fractional arc length of each side of the airfoil and G_j are the mode amplitudes, that are defined as design variables. 160 design variables are used to control the airfoils shapes at 8 wing spanwise positions. The third group includes the design variables defining the wing box structure. The thickness of the wing box four equivalent panels in 10 spanwise positions are defined as design variables, 40 in total. As mentioned earlier the aircraft fuel weight is defined as the objective function. The fuel weight is a function of the aircraft total weight, which is a function of the fuel weight. Also for wing structural analysis the aircraft MTOW is required which is a function of the fuel weight and wing structural weight. So in order to avoid any iteration during the optimization two surrogate variables for aircraft fuel weight and maximum take-off weight are added to the design vector as the fourth group of the design variables.

The aerostructural optimization is subject to several constraints. A series of constraints are used to avoid any structural failure. These constraints are define based on different load cases, which are determined using the aircraft flight envelope. Reference (Dillinger 2014) shows the flight envelope of the A320 aircraft. Using those data six load cases are selected for aircraft structural analysis and optimization as shown in Table 1. Load cases number 1 to 3 are used for analyzing the wing box failure. Depending on the load case (positive or negative load factor) the upper and lower panels can be under tension or compression. and the spars webs are

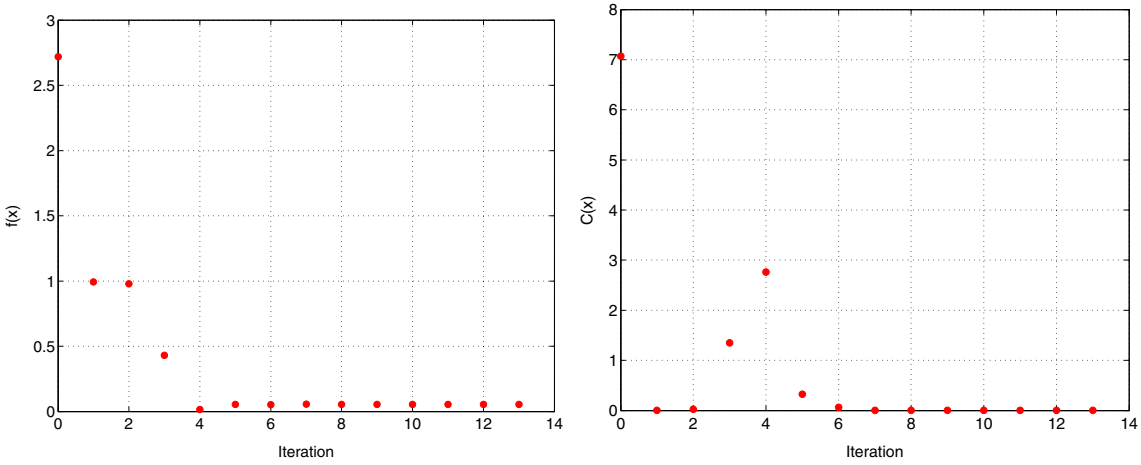

(a) Objective function (b) Maximum constraint violation.

Fig. 7 History of the analytical test case optimization

experiencing shear loads. All these different scenarios are taken into account. Load case number 4 is used to simulate fatigue in the wing lower panel and the load case number 5 is used to simulate the aileron effectiveness. Load case 6 is used for wing drag prediction during the cruise.

In order to reduce the total number of the constraints on structural failure, the Kresselmeier-Steinhauser (KS) function (Kreisselmeier and Steinhauser 1980) is used to aggregate the constraints, as follows:

$$KS[g(x)] = g_{max}(x) + \frac{1}{\rho_{KS}} ln \left[\sum_{j=1}^{m} e^{\rho_{KS}(g_j(x) - g_{max}(x))} \right] \tag{14}$$

where g_{max} is the maximum of all constraints. The parameter ρ_{KS} has been set to 50 as suggested by Poon and Martins (2007). All the failure constraints due to the 5 load cases are aggregated into 22 constraints using the KS function. A constraint is defined to keep the aircraft roll moment due to aileron deflection ($L_\delta = dL/d\delta$) higher or equal to the L_δ of the original wing. Another constraint is used to keep the wing loading lower or equal to the wing loading of the initial wing. Finally two consistency constraints are defined for the two surrogate design variables. The wing aerostructural optimization is formulated as follows:

$$\begin{aligned}
min \quad & W^*_{fuel}(X) \\
& X = [C_r, b, \lambda, \Lambda, \epsilon_{kink}, \epsilon_{tip}, G_i, t_{u_j}, t_{l_j}, t_{fs_j}, t_{rs_j}, \\
& W^*_{fuel}, MTOW^*] \quad i = 1..160, \quad j = 1:10 \\
s.t. \quad & \text{KS}_{\text{failure}_k} \leq 0 \quad k = 1..22 \\
& \frac{L_{\delta_0}}{L_\delta} - 1 \leq 0 \\
& \frac{MTOW/S_w}{MTOW_0/S_{w_0}} - 1 \leq 0 \\
& \frac{W_{fuel}}{W^*_{fuel}} - 1 = 0 \\
& \frac{MTOW}{MTOW^*} - 1 = 0 \\
& X_{lower} \leq X \leq X_{upper}
\end{aligned} \tag{15}$$

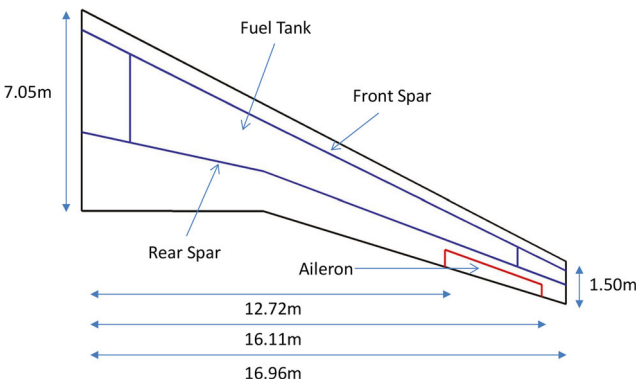

Fig. 8 Planform and wing box dimensions

Table 1 Load cases for wing aerostructural optimization

Load case	type	H [m]	M	n [g]	q [Pa]
1	pull up	7500	0.89	2.5	21200
2	pull up	0	0.58	2.5	23900
3	push over	7500	0.89	–1	21200
4	gust	7500	0.89	1.3	21200
5	roll	4000	0.83	1	29700
6	cruise	11000	0.78	1	10650

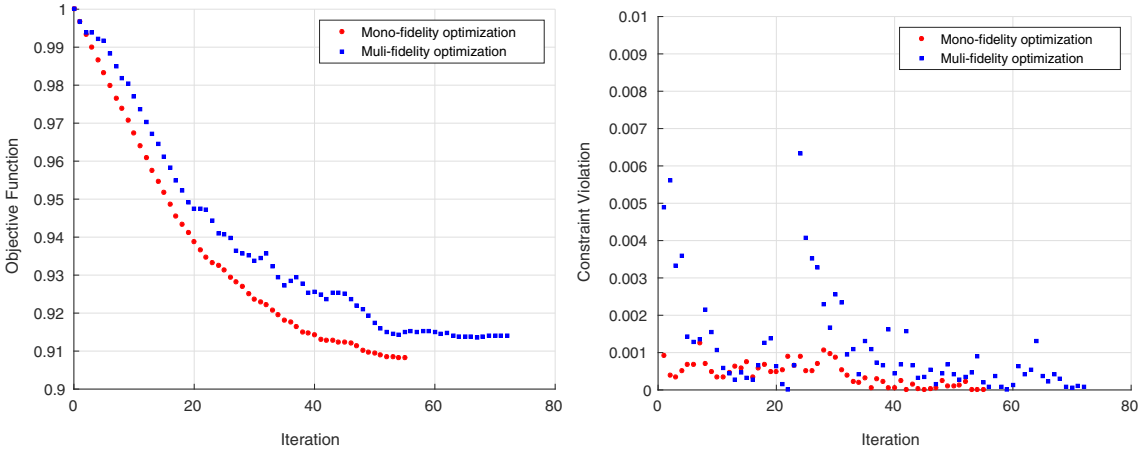

(a) Objective function

(b) Maximum constraint violation.

Fig. 9 Optimization history of the wing aerostructural optimization

4.2 Aerostructural optimization using the trust region filter-SQP method

In the first step a mono-fidelity optimization was performed. In that approach the aerostructural analysis method presented in Section 2 is used to predict the elastic wing drag and deformation. All the inequality constraints in (15) are changed to equality constraints by using slack variables. In total 24 slack variablesare added to the design vector. Besides, a series of bounds are defined to keep the values of these variables positive or zero.

In the second step a multi-fidelity optimization has been performed. March and Willcox (2012) modified the composite step filter method presented by Conn et al. (2000) to be used in a multi-fidelity optimization. The same approach as suggested by March and Willcox is used here to modify Algorithm 2 to be used for multi-fidelity optimization. In the modified algorithm, the Q3D aerodynamic analysis (connected with the FEM) is used as the low fidelity model and the MATRICS-V CFD code is used as the high fidelity tool. MATRICS-V is a 3D CFD code, which provides more accurate results than the Q3D method, but the computational time of running MATERICS-V is higher than Q3D. Besides, no analytical sensitivity analysis method is implemented in MATRICS-V. The MATRICS-V has been used for aerodynamic optimization using finite differencing for sensitivity analysis (Elham and van Tooren 2014) with limited number of design variables. However increasing the number of design variables and coupling the aerodynamic solver with a FEM for fully coupled aerostructural optimization, makes the use of finite differencing almost impossible. Therefore in the current research the low-fidelity aerostructural analysis tool is used to generate the TRQP, since that tool can compute the required sensitivities using analytical methods. Then the filter is applied based on the results of the MATRICS-V code. The drag predicted using the low fidelity model is calibrated using the results of the high fidelity model. Three calibration factors are defined for three different drag components (the induced drag, C_{D_i}, the pressure drag, C_{D_p},and the friction drag, C_{D_f}) as follows:

$$
\begin{aligned}
k_{cd_i} &= \frac{C_{D_{i_{\text{high}}}}}{C_{D_{i_{\text{low}}}}} \\
k_{cd_p} &= \frac{C_{D_{p_{\text{high}}}}}{C_{D_{p_{\text{low}}}}} \\
k_{cd_f} &= \frac{C_{D_{f_{\text{high}}}}}{C_{D_{f_{\text{low}}}}}
\end{aligned}
\tag{16}
$$

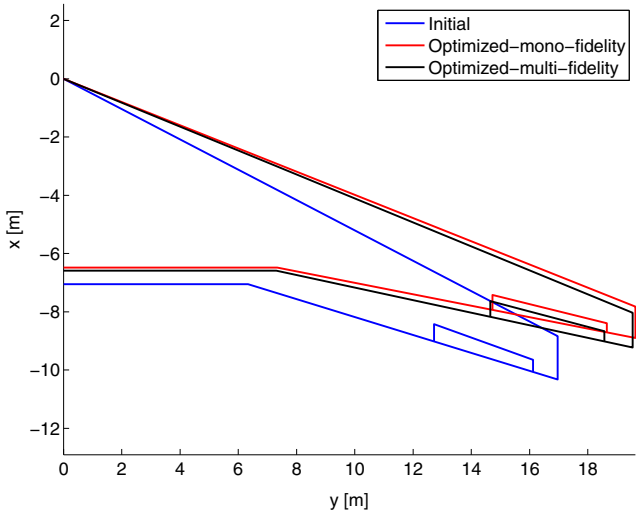

Fig. 10 Planform shapes of the initial and the optimized wings

Algorithm 3 Multi-fidelity trust region filter-SQP method

1: Choose x_0, Δ_0, Δ_{max}, Δ_{min}, η_1, η_2, γ_0, γ_1, γ_ϑ, k_ϑ
2: Initialize the Hessian as $H_0 = I$
3: Compute the value and the gradient of the objective function and the constraints using the low fidelity tool.
4: Solve the trust region quadratic programming (TRQP) to find s:

$$\begin{aligned} \text{minimize} \quad & m_k(s) = \frac{1}{2}\, s^T H(x_k)\, s + g(x_k)^T s \\ s.t. \quad & c(x_k) + A(x_k)s = 0 \\ & |s| \le \Delta_k \end{aligned}$$

5: If the TRQP does not have a feasible solution, then solve the restoration problem:

$$\text{minimize} \quad \vartheta_{low}(x_k + s) \equiv \|c(x_k + s)\|$$

6: Evaluate the objective function, the constraints and their derivatives at $x_k + s$ using the low fidelity method. Also evaluate the objective function and constraints using the high fidelity method at $x_k + s$.
7: Check if the new point is acceptable to the filter, i.e. if:

$$\begin{aligned} & f(x_k + s_k) < f_j - \gamma_\vartheta \vartheta_{high}(x_k + s_k) \quad \text{or} \\ & \vartheta_{high}(x_k + s_k) < (1 - \gamma_\vartheta)\vartheta_{high_j} \quad \text{for all } (f_j, \vartheta_{high_j}) \in \mathcal{F} \end{aligned}$$

where ϑ_{high} is the norm of the high fidelity constraints.
8: If $x_k + s_k$ is not acceptable to the filter, then set $x_{k+1} = x_k$ and $\Delta_{k+1} = min(\Delta_{min}, \gamma_0 \Delta_k)$ and go to 4.
9: If $x_k + s_k$ is acceptable to the filter and:

$$\begin{aligned} & m_k(x_k) - m_k(x_k + s_k) < k_\vartheta \vartheta^2_{high_k} \quad \text{and} \\ & \rho_k \equiv \frac{f(x_k) - f(x_k + s_k)}{m_k(x_k) - m_k(x_k + s_k)} \ge \eta_1 \end{aligned}$$

then set $x_{k+1} = x_k + s_k$, update the Hessian using i.e. the BFGS method, update the calibration factors of the low fidelity model based on the results of the high fidelity model and continue, else set $x_{k+1} = x_k$ and $\Delta_{k+1} = min(\Delta_{min}, \gamma_0 \Delta_k)$ and go to 4.
10: Add F_k and ϑ_{high_k} to the filter, remove the dominated pairs and update the trust region radius as follows:

$$\Delta_{k+1} = \begin{cases} \Delta_k & \text{if } \rho_k \in [\eta_1, \eta_2), \\ max(\Delta_{max}, \gamma_1 \Delta_k) & \text{if } \rho_k \ge \eta_2. \end{cases}$$

11: If the optimization has not converged go to 3.

After each iteration, if the new point is acceptable to the filter, the calibration factors are updated and the next iteration is performed. This guarantees that at the end of the optimization the drag predicted by the low fidelity model is the same as the drag predicted by the high fidelity model. This procedure is summarized in Algorithm 4. Since a surrogate variable is used for the aircraft fuel weight, which is the objective function, the variable level of fidelity does not affect the objective function. The value of the objective function is always the value of the surrogate fuel weight in the design vector. However the actual fuel weight is computed inside the constraint function in order to generate the consistency constraint on the fuel weight. Therefore two different values of the consistency constraint on the fuel weight and also the MTOW (which is a function of the fuel weight) are computed, one using the drag computed by the low fidelity model and one by using the drag predicted by the high fidelity model. The trust region filter-SQP method algorithm used for such a multi-fidelity optimization is shown in Algorithm 3.

Algorithm 4 Multi-fidelity wing aerostructural optimization method

1: Choose x_0, Δ_0, Δ_{max}, Δ_{min}, η_1, η_2, γ_0, γ_1, γ_ϑ, k_ϑ
2: Choose initial values of k_{cd_i}, k_{cd_p}, k_{cd_f} (these values can be 1 at the begining of the optimization)
3: Initialize the Hessian as $H_0 = I$
4: Run FEMWET to compute the value and the gradient of the objective function and the constraints.
5: Use the outputs of FEMWET to solve the trust region quadratic programming as shown in Algorithm 3.
6: If the TRQP does not have a feasible solution, then solve the restoration problem as shown in Algorithm 3.
7: Run FEMWET for $x_k + s$ to compute the objective function and the constraints as well as the wing deformation and different drag components.
8: Run MATRICS-V for $x_k + s$ using the wing deformed shape computed by FEMWET to evaluate the values of the different drag components.
9: Generate the filter using the outputs of MATRICS-V. Check if the new point is acceptable by the filter as shown in Algorithm 3.
10: If $x_k + s_k$ is not acceptable to the filter, then set $x_{k+1} = x_k$ and $\Delta_{k+1} = min(\Delta_{min}, \gamma_0 \Delta_k)$ and go to 5.
11: If $x_k + s_k$ is acceptable to the filter, i.e. all the conditions shown in step 9 of Algorithm 3 are satisfied, then set $x_{k+1} = x_k + s_k$, update the Hessian using i.e. the BFGS method, and compute the new values of the calibration factors k_{cd_i}, k_{cd_p}, k_{cd_f}.
12: Add F_k and ϑ_{high_k} to the filter, remove the dominated pairs and update the trust region radius as shown in Algorithm 3.
13: If the optimization has not converged go to 4.

As mentioned before in the TRQP, instead of ℓ_2 or ℓ_∞, a bound around the absolute value of s is defined. So Δ in TRQP is a vector with the same length as s. It helps to define different values of Δ for different design variables. As one can see in (15) different groups of design variables are used for a wing aerostructural optimization. Although all the design variables are normalized to have the same order of magnitude, defining the same trust region radius

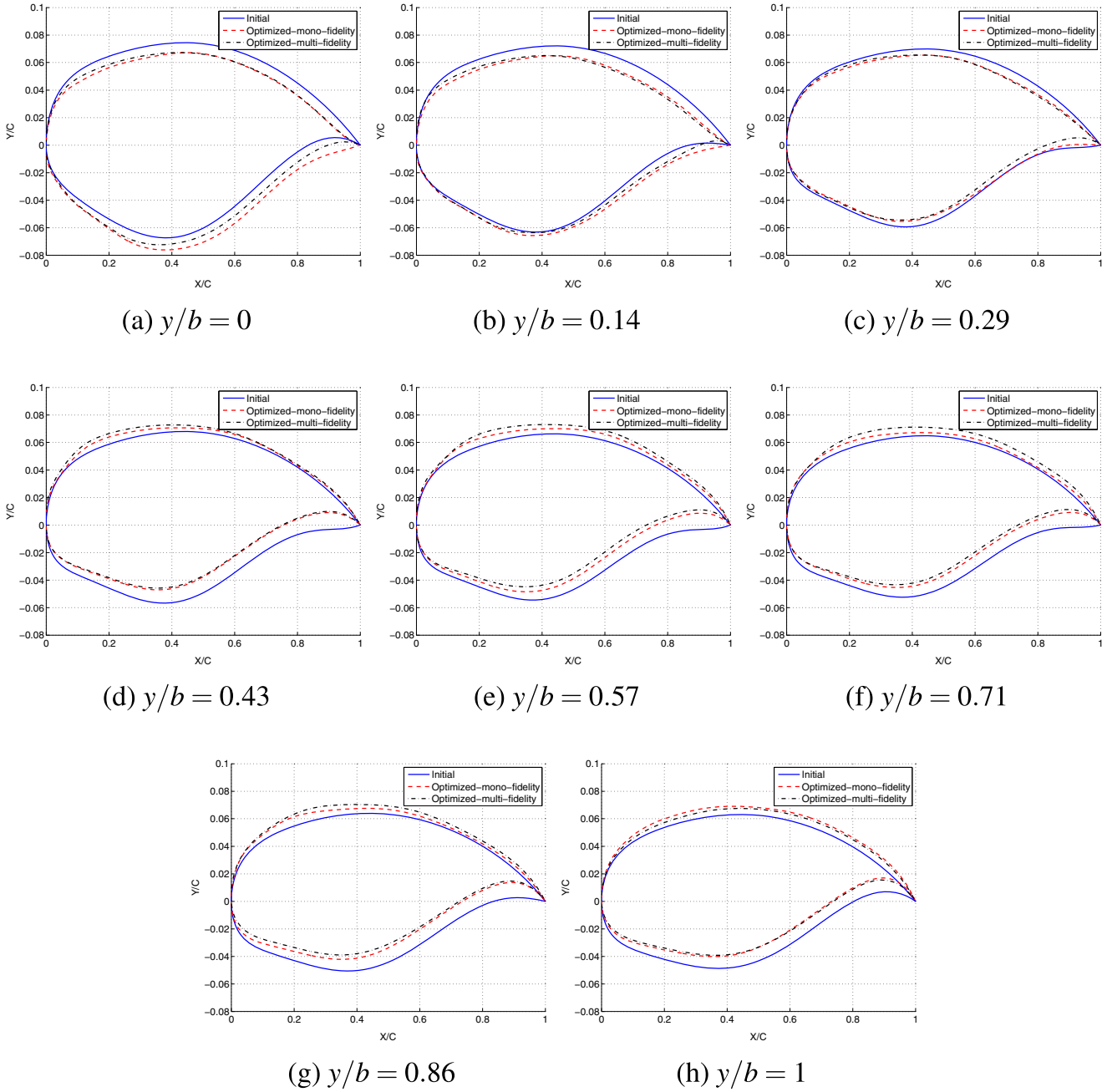

(a) $y/b = 0$ (b) $y/b = 0.14$ (c) $y/b = 0.29$

(d) $y/b = 0.43$ (e) $y/b = 0.57$ (f) $y/b = 0.71$

(g) $y/b = 0.86$ (h) $y/b = 1$

Fig. 11 The shape of the airfoils is several spanwise positions

for all of them does not seem logical. For example assuming the trust region radius allows 10 percent change in the design variables ($\Delta = 0.1$ for a design vector normalized with the initial values of the design variables). The effect of 10 % change in the thickness of the wing box skin at wing tip on the aircraft fuel weight is not the same as the effect of 10 % change in the aircraft MTOW on the aircraft fuel weight. By defining Δ as a vector, some design variables are allowed to have a larger change and some are more tightly limited. Selecting the proper values of Δ for different design variables is a challenge by itself. As mentioned, the value of Δ should be determined based on the sensitivity of the objective function and constraints with respect to the design variables. For those variables that have higher influence on the objective function a lower value for Δ should be used. In this case the design variables are categorized into four groups. The first group includes the design variables defining the wingbox structure. The second group includes the variables defining the airfoils geometry. The variables defining the wing planform geometry are categorized into the third group. And finally the variables defining the aircraft MTOW and the aircraft fuel weight are in the fourth

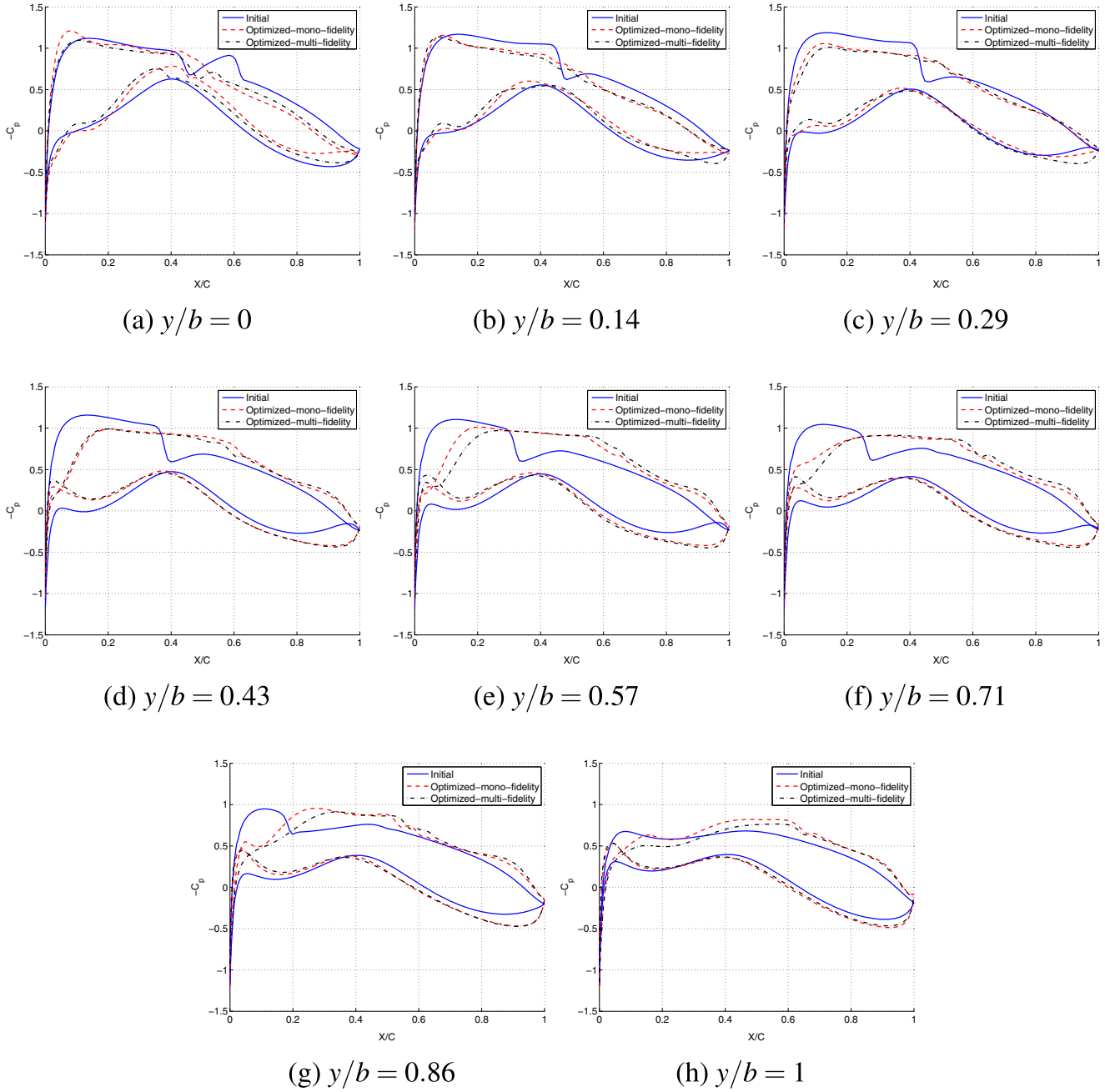

(a) $y/b = 0$ (b) $y/b = 0.14$ (c) $y/b = 0.29$

(d) $y/b = 0.43$ (e) $y/b = 0.57$ (f) $y/b = 0.71$

(g) $y/b = 0.86$ (h) $y/b = 1$

Fig. 12 Pressure distribution on airfoils in several spanwise positions

group. Defining the value of Δ, the trust region radios of the first and second group of the variables are set equal to Δ, the trust region radios of the third group is set to $\Delta/2$, and the trust region radios of the fourth group is set to $\Delta/3$.

The history of the both mono-fidelity and multi-fidelity optimization is shown in Fig. 9. Figure 10 shows the planform of the initial wing compared to the planform of the optimized wing using both the mono-fidelity and the multi-fidelity optimizations. The shape of the airfoils in several spanwise position and the pressure distribution on those airfoils are shown in Figs. 11 and 12 respectively. The characteristics of the optimized aircraft are summarized in Table 2.

From Table 2 one can observe that the multi-fidelity optimization resulted in slightly less fuel weight reduction (about 0.7 % less than mono-fidelity optimization). The drag of the wing optimized using the multi-fuidelity approach is slightly higher than the drag of the wing optimized using only the low fidelity model. It can be explained

Table 2 Characteristics of the initial and the optimized aircraft

	MTOW	W_{fuel}	W_{wing}	C_D
Initial	1	1	1	1
Optimized - mono-fidelity	0.9813	0.9053	1.0370	0.7598
Optimized - multi-fidelity	0.9847	0.9120	1.0520	0.7830

by looking at Fig. 4, showing that the low fidelity model slightly underestimates the drag comparing to the high fidelity model. The wing optimized using the multi-fidelity approach has slightly higher sweep than the one optimized using the mono-fidelity method, therefore it has slightly higher wing structural weight. In general the results of the multi-fidelity optimization are more realistic, since a more accurate drag analysis is used. However the results of the mono-fidelity optimization are quite similar to the results of the multi-fidelity optimization, that indicates a good level of accuracy of the low fidelity model. It should also be noted that the mono-fidelity optimization was about 4 times faster than the multi-fidelity optimization.

In both cases the optimizer moved toward a larger wing span and a lower leading edge sweep. The larger span results in a lower induced drag, but a higher wing structural weight. Lower sweep, on the other hand, results in a lower structural weight, but may increase the wave drag. However the optimizer managed to modify the airfoil shapes to eliminate the shock wave from the surface of the optimized wings, see Fig. 12.

The constraint on the aileron effectiveness is usually an active constraint in wing aeroelastic optimization. In fact to achieve higher aileron effectiveness, and consequently a higher value of L_δ, a higher wing stiffness (mainly torsional stiffness) is required for a given wing and aileron geometry. Increasing the torsional stiffness results in a higher structural weight. The study of Elham and van Tooren (2016a) showed that the wing structural weight increases quadratically by increasing the required value for aileron effectiveness. The optimizer in this research, both in the mono-fidelity and multi-fidelity cases, moved toward a more flexible wing to reduce the wing structural weight. The initial wing has a tip vertical deflection of 1.48m and tip twist of -3.8 degrees under 2.5g pull up load, while the optimized wing (using multi-fidelity method) has a tip vertical deflection of 1.77m and tip twist of -3.9 degrees. The aircraft roll requirement was satisfied by increasing the aileron arm and the aileron surface (both were resulted from a larger span). The larger aileron area and arm allowed to keep the value of L_δ higher than the required (4.04×10^4 for the optimized wing vs 3.80×10^4 for the initial wing) with a lower value of the aileron effectiveness (0.43 for the optimized wing vs 0.53 for the initial wing), that resulted from a lower wing stiffness.

5 Conclusions

In this research a trust region filter-SQP method is used for wing multi-fidelity aerostructural optimization. This algorithm allows to combine a lower fidelity model, that predicts the sensitivity of the objective function and the constraints, with a higher fidelity model, that is more accurate but more expensive to be executed. The low fidelity model is used to generate the TRQP subproblem. The high fidelity model is used to generate the filter and also to calibrate the results of the low fidelity model. Using that approach a high fidelity CFD tool that does not provide the sensitivities, can be used for a gradient based optimization. In addition to that, the aerodynamic solver is coupled with a structural solver for a fully coupled aerostructural optimization.

This research showed that a high fidelity aerodynamic solver can be used in an optimization without a need for high performance computer clusters. This reduces the cost and time of the optimization and makes high fidelity optimization feasible using ordinary computers.

A mono-fidelity as well as a multi-fidelity wing aerostructural optimization have been performed using the proposed algorithm. The results showed about 9 % reduction in the aircraft fuel weight. The optimizer found the optimum planform shape, airfoil shape as well as the wing box structure to achieve that amount of reduction in the fuel weight.

In this study only a high fidelity aerodynamic solver was combined with the low fidelity aerostructural analysis tool. As the next step a high fidelity FEM can be combined with the low fidelity tool as well. In that approach both the aerodynamic and structural analysis can be performed using two different levels of fidelity. There will be no need for modifying the proposed algorithm. The same algorithm can be used, but this time the constraints related to the wing structure will be computed using two different tools.

References

Alexandrov NM, Lewis RM, Gumbert CR, Green LL, Newman PA (2001) Approximation and model management in aerodynamic optimization with variable-fidelity models. J Aircr 38(6):1093–1101

Berci M, Toropov VV, Hewson RW, Gaskell PH (2014) Multidisciplinary multifidelity optimisation of a flexible wing aerofoil with reference to a small UAV. Struct Multidiscip Optim 50:683-699

Conn AR, Gould NIM, Toint PL (2000) Trust-Region Methods. MPS-SIAM Series on Optimization, Philadelphia, p 959

Dillinger JKS (2014) Statis Aeroelastic Optimization of Composite Wings with Variable Stiffness Laminates. PhD thesis, Delft University of Technology, Delft, The Netherlands

Elham A (2015) Adjoint quasi-three-dimensional aerodynamic solver for multi-fidelity wing aerodynamic shape optimization. Aerosp Sci Technol 41:241–249

Elham A, van Tooren MJL (2014) Effect of wing-box structure on the optimum wing outer shape. The Aeronautical Journal 118(1199):1–30

Elham A, van Tooren MJL (2016) Tool for preliminary structural sizing, weight estimation, and aeroelastic optimization of lifting surfaces. In: Proceedings of IMechE Part G: J Aerospace Engineering, vol 230, pp 280–295

Elham A, van Tooren MJL (2016) Coupled Adjoint Aerostructural Wing Optimization Using Quasi-Three-Dimensional Aerodynamic Analysis. Struct Multidisc Optim 54:889-906. doi:10.1007/s00158-016-1447-9

Fletcher R, Leyffer S (2002) Nonlinear programming without a penalty function. Math Program Ser A 91:239–269

Fletcher R, Leyffer S, Toint PL (2002) On the convergence of a filter-SQP algorithm. SIAM J Optim 13(1):44–59

Kennedy GJ, Martins JRRA (2014) A parallel aerostructural optimization framework for aircraft design studies. Struct Multidiscip Optim 50(6):1079–1101

Kenway GKW, Martins JRR (2014) Multipoint high-fidelity aerostructural optimization of a transport aircraft configuration. J Aircr 21(1):144–160

Kenway GKW, Kennedy GJ, Martins JRRA (2014) Scalable parallel approach for High-Fidelity Steady-State aeroelastic analysis and adjoint derivative computations. AIAA J 52(5)

Kreisselmeier G, Steinhauser R (1980) Systematic control design by optimizing a vector performance indicator. In: Cuenod MA (ed) IFAC Symposium on computer aided design of control systems. Pergamon Press, Oxford

March A, Willcox K (2010) Convergent multifidelity optimization using Bayesian model calibration. In: 13th AIAA/ISSMO multidisciplinary analysis and optimization conference, 13-15 September 2010, Fort Worth, TX, USA, AIAA 2010-9198

March A, Willcox K (2012) A Robust approach to aerostructural design. In: 3rd aircraft structural design conference. Royal Aeronautical Society, Delft

Martins JRRA, Alonso JJ, Reuther JJ (2005) A coupled-adjoint sensitivity analysis method for high-fidelity aero-structural design. Optim Eng 6:33–62

Meredith PT (1993) Viscous phenomena affecting high-lift systems and suggestions for future CFD development. AGARD TR-94-18415-04–01

Niu MCY (1997) Airframe stress analysis and sizing. Conmilit Press Ltd, Hong Kong

Nocedal J, Wright SJ (2000) Numerical Optimization. Springer, New York, p 664

Obert E (2009) Aerodynamic design of transport aircraft. IOS press, Amsterdam, p 638

Poon NMK, Martins JRRA (2007) An adaptive approach to constraint aggregation using adjoint sensitivity analysis. Struct Multidisc Optim 34:61–73

Rajnarayan D, Haas A, Kroo I (2008) A Multifidelity Gradient-Free Optimization Method and Application to Aerodynamic Design. In: 12th AIAA/ISSMO Multidisciplinary Analysis and Optimization Conference 10 - 12 September 2008, Victoria, British Columbia Canada, AIAA Paper No. 2008-6020

Roskam J (1986) Airplane design, Part I: Preliminary sizing of airplanes. DARcorporation, Lawrence, Kan

Rump SM (1999) INTLAB - Interval Laboratory. In: Developments in Reliable Computing, Kluwer, Dordrecht, pp 77–104

Torenbeek E (2013) Advanced Aircraft Design, Conceptual Design, Analysis and Optimization of Subsonic Civil Airplanes. Wiley, West Sussex, p 410

van Dam C (2003) Aircraft design and the importance of drag prediction. In: CFD-Based Aircraft Drag Prediction and Reduction, vol 2, pp 1-37. von Karman Institute for Fluid Dynamics, Rhode-St-Genese, Belgium

Vanderplaats GN (2007) Multidisciplinary Design Optimization, Monterey. Vanderplaats Research and Development Inc

van der Wees AJ, van Muijden J, van der Vooren J (1993) A Fast and Robust Viscous-Inviscid Interaction Solver for Transonic Flow About Wing/Body Configurations on the Basis of Full Potential Theory. AIAA Paper 1993–3026